CHEMICAL ENGINEERING TRANSACTIONS
VOL. 71, 2018
A publication of AIDIC
The Italian Association of Chemical Engineering
Online at www.aidic.it/cet
Guest Editors: Xiantang Zhang, Songrong Qian, Jianmin Xu
Copyright © 2018, AIDIC Servizi S.r.l.
ISBN 978-88-95608-68-6; **ISSN** 2283-9216
DOI: 10.3303/CET1871203

Analysis of Discharge Reaction Process and Study on Influencing Factors of New Energy Battery Based on Computer Simulation Technology

Yushuo Tan

Shijiazhuang Posts And Telecommunications Technical College, Shijiazhuang 050021, China
tanys@163.com

NEBs (New Energy Batteries) have some advantages that the fossil energy can not match. Dye-Sensitized Solar Battery (DSSB) as a state-of-art technology will not be directly measured for its intrinsic parameters due to its immature technology. Based on the Computer Simulation Technology (CST), this paper integrates the electrochemical and optical processes of DSSBs into account, and conducts a survey on how the externalities are subject to optical properties. The findings show that: screen printing film can prepare the DSSBs with good properties; it is found by simulation that the driving force of the battery attributes to the uneven diffusion of electron concentration distribution caused by chemical action, and the electric field strength and average electron density in open circuit are higher than that in the short circuit. With the CST, battery output properties can be simulated regardless of the internal transport mechanism of the charge. The study in this paper provides the clues to measuring the intrinsic parameters of NEBs.

1. Introduction

Along with the sharp increase of the world's population, fossil energy tends to be depleted. There is a greater demand for new energy sources such as solar energy and wind energy (Miranda et al., 2018). As a renewable new energy source, solar energy has the advantages the fossil energy has no equal, for instance, it is inexhaustible and does not break the earth's heat balance and avails to protect the ecological environment (Khayyam et al., 2013; Thiedmann et al., 2011). By far, there are newly developed monocrystalline silicon, polycrystalline silicon thin film, and amorphous silicon thin film solar batteries. In order to scale up the development of poly-compound thin film solar batteries, the models made from different materials have been developed one after another (Wang et al., 2017; Sahraei et al., 2012). The indicators for evaluating solar batteries include photoelectric conversion efficiency, short-circuit current, open circuit voltage, total battery efficiency, and fill factor, etc. (Shen and Chirwa, 2018).

The new DSSB consists of counter electrode, electrolyte solution, dye, nano-titanium dioxide porous membrane, and conductive substrate (Esfahanian et al., 2015). We use the nanometer TiO_2 film adsorb the photosensitive dye and take it as the NEB anode assembled with the cathode of the film platinum, and then the electrolyte is dripped between the two poles to form a novel DSSB (Lin and Tang, 2016). The optical trapping can be finished by dye molecules. After absorbing the photons, the dye molecules in the excited state generate charge transfer from the central ion to the ligand. Then electrons are injected into the TiO_2 conduction band via the ligand and transported to photoanode via the porous TiO_2 film, further to the counter electrode from the external circuit via the loads. The dye molecules are reduced by the iodide ions in the electrolyte to achieve charge separation (Zhou et al., 2018; Mao et al., 2016). Based on CST, this paper integrates the electrochemical and optical processes of DSSBs into account, and makes a survey on how the optical properties affect its externalities.

Please cite this article as: Tan Y., 2018, Analysis of discharge reaction process and study on influencing factors of new energy battery based on computer simulation technology, Chemical Engineering Transactions, 71, 1213-1218 DOI:10.3303/CET1871203

2. Analysis of discharge process of DSSB

2.1 Development technology for DSSB

In the DSSB, nanocrystalline TiO_2 film, as an intermediate bridge between dyes and conductive films, has the function of fixing dyes (Tang et al., 2012). Formulas 1~ 3 represent the process for preparing a nanocrystalline TiO_2 film by the powder coating, screen printing, electrochemical deposition, or the like, and the first two are commonly used (Liu et al., 2014). As shown in Figure 1, a photocurrent-voltage curve is plotted out for a battery prepared by different film preparation methods. It is observed that the open circuit photocurrents of the battery prepared by the screen printing and the powder coating methods are 17.29mA/cm^2 and 16.76 mA/cm^2, respectively, and the open circuit photovoltages of both are 540mV and 500mV, respectively. As shown in Table 1, the behaviors of batteries produced by the screen printing and powder coating differ from each other. By contrast, the battery prepared by the screen printing method has a higher short-circuit photocurrent, open circuit photovoltage, photoelectric conversion efficiency and fill factor than that by the powder coating method; the power coating has a simpler preparation process, controllable particle size, but the membrane obtained by the screen printing can get a larger specific surface area and a better porous property (Gallaway et al., 2016; Rincón et al., 2018).

$$nTi(OR)_4(g)+4nH_2O(g)=nTi(OH)_4(s)+4nROH(g) \quad (1)$$

$$nTi(OR)_4(s)=nTiO_2\cdot H_2O(s)+nH_2O(g) \quad (2)$$

$$nTiO_2\cdot H_2O(s)= nTiO_2+nH_2O(s) \quad (3)$$

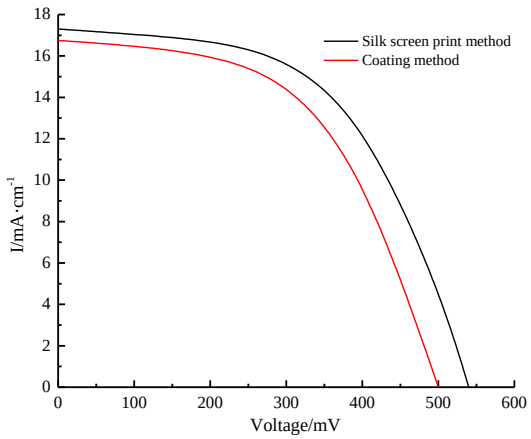

Figure 1: Photocurrent-voltage curves of batteries prepared by different membrane methods

Table 1: Difference in performance between screen printing and powder coating

Coating technology	Screen printing	Coating method
I_{sc}(mA/cm^2)	16.41	15.86
Voc(mV)	529	489
ff (%)	0.5567	0.5411
η(%)	5.18	4.51
Surface roughness	411.81	366.34
Film thickness(m)	7.6	6.3

2.2 Charge transfer and recombination in dye-sensitized solar cells

As a new energy battery, the DSSB has three charge transfer processes, i.e. photo-electric generation, electron-pair separation and circuit transmission (Ruggeri et al., 2016). Under illumination, the sensitized TiO_2 film is excited by photon excitation on the film. At this time, charge transfer occurs in the ligand. Electrons are injected into the TiO_2 conduction band via the ligand, enrich on the conductive glass and generate the working current via external circuit. The whole battery completes one cycle to achieve the process that the raw material loses electrons to the ground state, and receives electrons for proceeding reduction. The DEEB charge transfer and recombination process runs like this: dye excitation - photocurrent generation - dye reduction - electrolyte reduction - electron recombination - dark current - return to the ground state.

3. Computer simulation on electron transfer driving force in porous nanocrystal electrodes

3.1 Electron transfer driving force model

The solar photoelectron is injected into the TiO_2 conduction band, and the electrons diffuse to the substrate via the TiO_2 film. When the electrons deposited on the substrate satisfy the open circuit condition, the photovoltage generates. Then photocurrent generates under the short circuit condition of the photovoltage. Assume that N(x, t) represents the number of free electrons at x from the substrate, the Fermi level and current density Jn(x, t) of the nanocrystal network are shown in formulas 4 and 5, respectively:

$$E_{F,n}(x,t)-E_{F,n}^{ref}=-e[\psi(x,t)-\psi^{ref}]+kT\ln\frac{n(x,t)}{n^{ref}} \tag{4}$$

$$J_n(x,t)=\mu_n n(x,t)[-\frac{1}{e}\frac{\partial E_{F,n}(x,t)}{\partial x}] \tag{5}$$

Where: *e* represents the charge quantity; *k* represents the Boltzmann constant; μ_n represents the electron mobility.

If the electric field of driving force is ignored, the concentration of charges at x from the substrate is expressed in the form of Fick's first law, as shown in formulas 6 and 7:

$$n(x)-n(d)=\frac{\Phi(0)}{\alpha Dn}[\alpha x+e^{-\alpha d}-e^{-\alpha x}] \tag{6}$$

$$-\frac{1}{e}\frac{dE_{F,n}(x)}{dx}=\frac{kT}{e}\frac{1-e^{-\alpha x}}{\alpha x+e^{-\alpha d}-e^{-\alpha x}} \tag{7}$$

As shown in the formulas, the driving force is independent of the incident intensity and the diffusion coefficient, while the electron current only has a significant correlation with the electron mobility and the charge driving force. Further, it is considered how the driving force of electron diffusion is subjected to the light absorption depth. Existing studies show that there is a linear relationship between the driving force and the absorption depth. As the absorption depth increases, the relative highlight absorption is expressed as:

$$-\frac{1}{e}\frac{dE_{F,n}(x)}{dx}=\frac{kT}{e}\frac{\alpha x}{d(d-x)} \tag{8}$$

3.2 Driving force simulation and result analysis

In this driving force simulation test, the thickness of the nanocrystalline TiO_2 film is 1μm; the absorption depths take 1 and 10; the incident intensities are $10^{15}cm^2s^{-1}$ and 10^{16} cm^2s^{-1}, respectively, and the diffusion coefficient is $10^{-5}cm^2s^{-1}$. The relationship between the charge concentration and position is shown in Figure 2. It can be seen that electron concentration at the interface of the porous membrane of the electrolyte is zero, and near this interface, it has a linear relation with x, while at the porous interface of the substrate, it reaches the peak. When simulating, the Boltzmann constant takes 1.38×10^{23}J/K and the temperature is 300K. The relationship between the driving force and the position is shown in Figure 3. It can be clearly seen that the driving force fluid, absorption depth and driving force itself all get higher with the increase of the position x. Given that the driving force is susceptible to the electric field action, it is only necessary to multiply the coefficient greater than 1, and there is no substantial change in driving force.

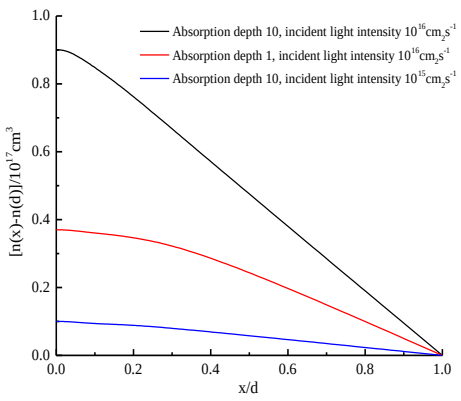

Figure 2: Schematic diagram of charge concentration and charge position

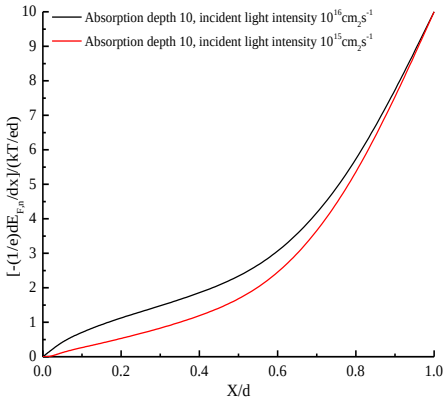

Figure 3: Schematic diagram of relationship between driving force and position

4. Computer Simulation on DSSB properties

4.1 Simulation model

The models used in the computer simulation process include both electrochemical and optical transmission models. In the process, the microscopic electric field in the battery needs to be neglected. Assume the electron generation rate is independent of the electron relaxation rate, the quantum yield is 1, and the carrier transport in the battery is shown in Formulas 9-11, and the quasi-one-dimensional model of dye-sensitized TiO_2 nanocrystalline solar battery is shown in Figure 4. When using an electrochemical model, the battery is regarded as a medium with thickness z, and containing carriers in the middle. Under light conditions, carriers' non-equilibrium distribution causes the generation of an electric field.

$$\frac{1}{e_0} j_e(x) = -D_e \frac{d}{dx} n_e(x) - \mu_e n_e(x) E(x) \tag{9}$$

$$\frac{1}{e_0} j_{I^-}(x) = -D_{I^-} \frac{d}{dx} n_{I^-}(x) - \mu_{I^-} n_{I^-}(x) E(x) \tag{10}$$

$$\frac{1}{e_0} j_c(x) = -D_c \frac{d}{dx} n_c(x) - \mu_c n_c(x) E(x) = 0 \tag{11}$$

In the optical transmission model, the beam is divided into parallel and diffused beams, assume that the nanocrystalline TiO_2 film is an isotropic non-luminance medium. A beam of light is incident in parallel from one side of the battery. After multiple reflections, a portion of the light enters the medium. The beam propagates via the medium to form diffused light. The other part is directly reflected out, and the following transmission equation can be obtained:

$$\frac{dI_c}{dx} = (k+s) I_c \tag{12}$$

$$\frac{dJ_c}{dx} = -(k+s) J_c \tag{13}$$

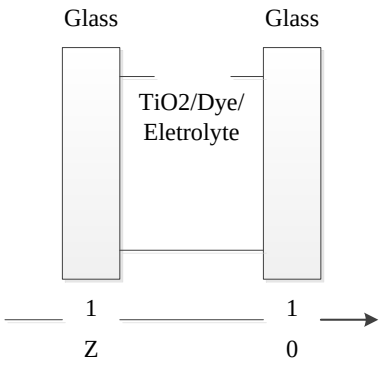

Figure 4: Schematic diagram of quasi-one-dimensional model of dye-sensitized TiO_2 nanocrystalline solar cells

4.2 Battery simulation results under standard parameters

As shown in Figure 5, it is the kinetic process of a DSSB, including the electron loss and dynamic balance processes in the battery, there are the excitation, transport and recombination in the computer simulation process. Computer simulation may analyze the changes in various parameters in the battery. Table 2 lists the standard parameters for some DSSBs, including electron relaxation rate constant, electron mobility, incident photon flux density, etc. Any parameter available is definite. As shown in Figure 6, the curve of battery output properties is given; simulated short-circuit current is 15.08 mA; open-circuit voltage is 680 V; the maximum power displayed in simulation process corresponds to 512.83 V, which can correctly reflect the working state of the battery. Figure 7 gives a distribution curve of the electric field intensity E in the battery. The electric field strength at the time of the open circuit is greater than that at the short circuit, that is, the voltage drop caused by the electric field kinetic action is less than 1 mV, which implies that the DSSB power generation mainly depends on chemical kinetics. Figure 8 is a distribution curve of the electron density in the battery. Since the electron relaxation rate is less at the time of short circuit, the average electron density in the open circuit is much higher than that in the short circuit.

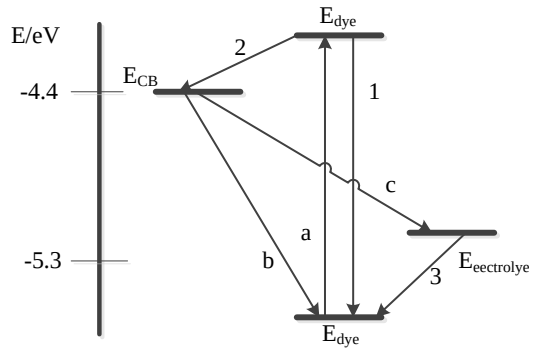

Figure 5: Kinetic process of dye-sensitized solar cells

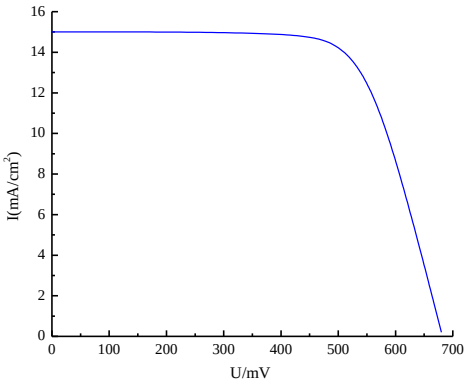

Figure 6: Battery output characteristic curve

Table 2: Standard parameters for dye-sensitized solar cells

Parameter name	Standard value
Electron relaxation rate constant	10^4S^{-1}
Electron mobility	$0.4cm^2/Vs$
Effective relative permittivity	60
Incident photon flux density	$90mW/cm^2$
Battery thickness	11μm
Battery area	$1cm^2$
Voidage	0.35

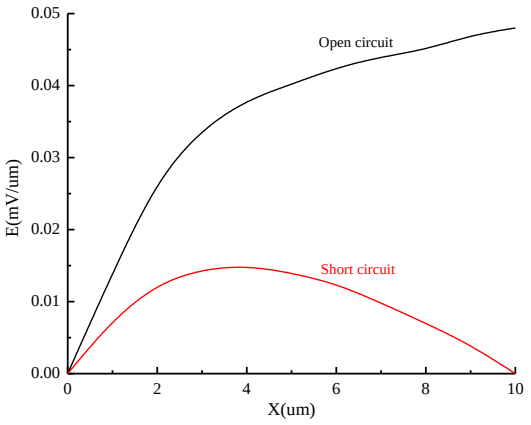

Figure 7: Distribution curve of electric field strength E in battery

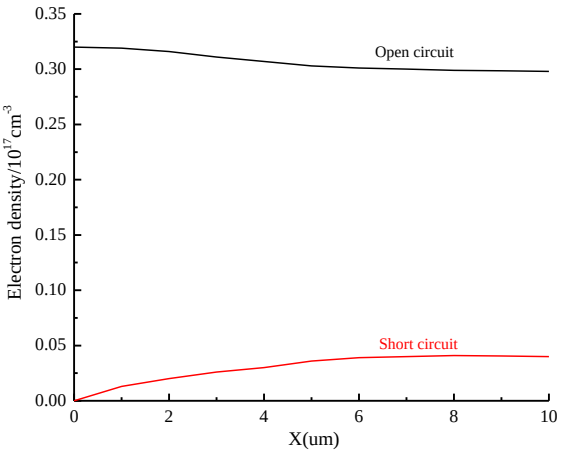

Figure 8: Electron density distribution curve in battery

5. Conclusion

Based on the CST, this paper integrates the electrochemical and optical processes of the DSSBs into account, and investigates how their externalities are subject to optical properties. The specific conclusions are drawn as follows:

(1) Under illumination, the sensitized TiO_2 film dye is excited by photons, and charge transfer occurs in the ligand. Electrons are injected into the TiO_2 conduction band via the ligand and enriched on the conductive glass. Then, they generate the working current via external circuit, and the whole battery finishes one cycle to achieve the process that the raw material loses electrons to the ground state, and receives the electrons to be restored.

(2) The concentration of electrons at the interface of the porous membrane of the electrolyte is zero. The concentration of electrons near it has a linear relation with x, and maximum electron concentration appears at the porous interface of the substrate.

(3) Power generation of DSSB depends on chemical kinetics. The electric field strength at the time of open circuit is higher than that at short circuit, so does its average electron density.

Acknowledgments

2017 Hebei science and technology program project establishment “The development and research of the intelligent newspapers and periodicals sorting system based on PDA control” Project number: 17214711.

References

Esfahanian V., Ansari A.B., Torabi F., 2015, Simulation of lead-acid battery using model order reduction, Journal of Power Sources, 279, 294-305, DOI: 10.1016/j.jpowsour.2014.12.149

Gallaway J.W., Hertzberg B.J., Zhong Z., Croft M., Turney D.E., Yadav G.G., 2016, Operando identification of the point of [mn 2] o 4, spinel formation during γ-mno 2, discharge within batteries, Journal of Power Sources, 321, 135-142, DOI: 10.1016/j.jpowsour.2016.05.002

Khayyam H., Abawajy J., Javadi B., Goscinski A., Stojcevski A., Bab-Hadiashar A., 2013, Intelligent battery energy management and control for vehicle-to-grid via cloud computing network, Applied Energy, 111(11), 971-981, DOI: 10.1016/j.apenergy.2013.06.021

Lin C., Tang A., 2016, Simplification and efficient simulation of electrochemical model for li-ion battery in evs, Energy Procedia, 104, 68-73, DOI: 10.1016/j.egypro.2016.12.013

Liu X., Wu J., Zhang C., Chen Z., 2014, A method for state of energy estimation of lithium-ion batteries at dynamic currents and temperatures, Journal of Power Sources, 270(3), 151-157, DOI: 10.1016/j.jpowsour.2014.07.107

Mao Y., Zhang J., Letaief K.B., 2016, Dynamic computation offloading for mobile-edge computing with energy harvesting devices, IEEE Journal on Selected Areas in Communications, 34(12), 3590-3605, DOI: 10.1109/JSAC.2016.2611964

Miranda D., Costa C.M., Almeida A.M., Lanceros-Méndez S., 2018, Computer simulation of the influence of thermal conditions on the performance of conventional and unconventional lithium-ion battery geometries, Energy,149, 262-278, DOI: 10.1016/j.energy.2018.02.026

Rincón L., Agualimpia B., Zafra G., 2018, Differential protein profiles of the lipolytic yeast candida palmioleophila under different growth conditions, Chemical Engineering Transactions, 64, 343, DOI: 10.3303/CET1864058

Ruggeri I., Arbizzani C., Soavi F., 2016, A novel concept of semi-solid, li redox flow air (o 2) battery: a breakthrough towards high energy and power batteries, Electrochimica Acta,206, 291-300, DOI: 10.1016/j.electacta.2016.04.139

Sahraei E., Hill R., Wierzbicki T., 2012, Calibration and finite element simulation of pouch lithium-ion batteries for mechanical integrity, Journal of Power Sources, 201(3), 307-321, DOI: 10.1016/j.jpowsour.2011.10.094

Shen N., Chirwa E.M.N., 2018, Biosorption and desorption potential of gold(iii) by freshwater microalgae scenedesmus obliquus as-6-1, Chemical Engineering Transactions, 64, DOI:10.3303/CET1864004

Tang A., Bao J., Skyllas-Kazacos M., 2012, Thermal modelling of battery configuration and self-discharge reactions in vanadium redox flow battery, Journal of Power Sources, 216(216), 489-501, DOI: 10.1016/j.jpowsour.2012.06.052

Thiedmann R., Stenzel O., Spettl A., Shearing P.R., Harris S.J., Brandon N.P., 2011, Stochastic simulation model for the 3d morphology of composite materials in li–ion batteries, Computational Materials Science,50(12), 3365-3376, DOI: 10.1016/j.commatsci.2011.06.031

Wang Z., Fan W., Liu P., 2017, Simulation of temperature field of lithium battery pack based on computational fluid dynamics, Energy Procedia, 105, 3339-3344, DOI: 10.1016/j.egypro.2017.03.764

Zhou F., Wu Y., Hu R.Q., Qian Y., 2018, Computation rate maximization in uav-enabled wireless powered mobile-edge computing systems, IEEE Transactions on Wireless Communications, 17(6), 4177-4190, DOI: 10.1109/TWC.2018.2821664